LECTURE 21: MICROSTRIP ANTENNAS – PART II

(Transmission-line model. Design procedure for a rectangular patch. Cavity model for a rectangular patch.)

1. Transmission Line Model – The Rectangular Patch

The TL model is the simplest of all, representing the rectangular patch as a parallel-plate transmission line connecting two radiating slots (apertures), each of width W and height h. In the figure below, z is the direction of propagation in the transmission line.

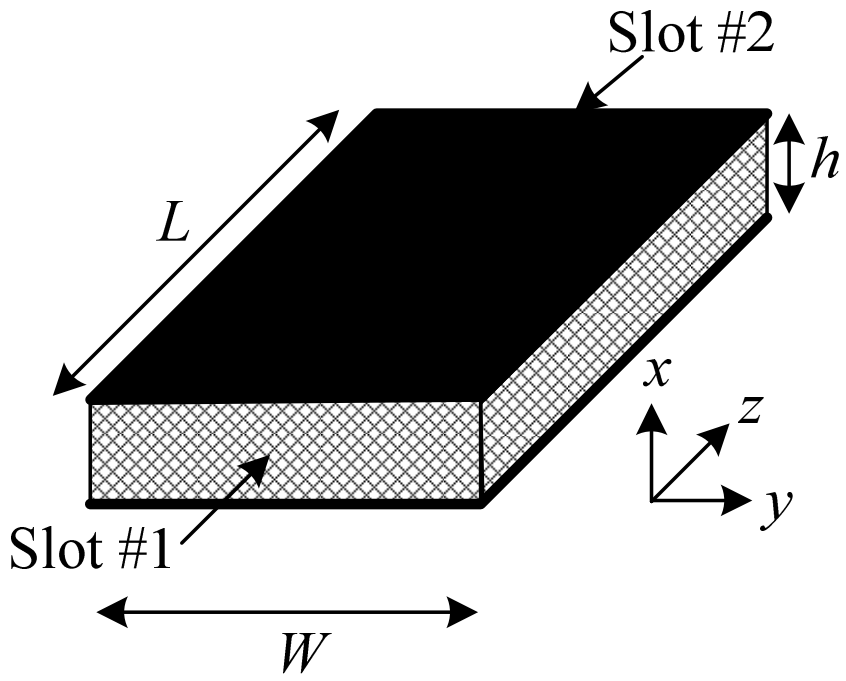

The TL model is not very accurate and lacks versatility as far as patch shapes are concerned. However, it gives a relatively good physical insight into the physics of the patch antenna and the field distribution for all TM_{00n} modes.

The slots represent very high-impedance terminations on both sides of the transmission line (almost an open circuit). Thus, the patch has highly resonant characteristics depending crucially on its length L along z. The resonant length of the patch, however, is not exactly equal to the physical length due to the ***fringing effect***. The fringing effect makes the effective electrical length of the patch longer than its physical length, $L_{eff} > L$. Thus, the resonance condition

$\beta^{(n)} L_{eff} = n \cdot \pi / 2$, $n = 1, 2, \ldots$, depends on L_{eff}, not L. A sketch of the **E**-field distribution for the first (dominant) resonant mode, $n = 1$, is shown in the figure below.

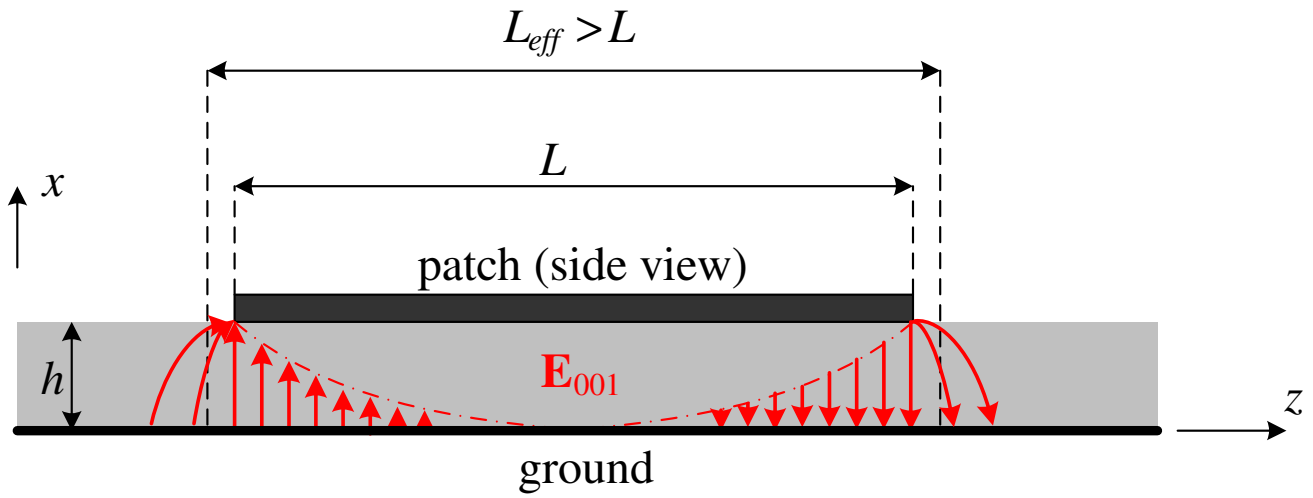

A. Computing the effective patch length

The effective length extension of the patch ΔL due to the edge effect at each radiating edge can be computed as:

$$\frac{\Delta L}{h} = 0.412 \frac{\left(\varepsilon_{r_{eff}} + 0.3\right)\left(\frac{W}{h} + 0.264\right)}{\left(\varepsilon_{r_{eff}} - 0.258\right)\left(\frac{W}{h} + 0.8\right)}. \qquad (21.1)$$

For the computation of $\varepsilon_{r_{eff}}$, see previous Lecture. The effective length is

$$L_{eff} = L + 2\Delta L. \qquad (21.2)$$

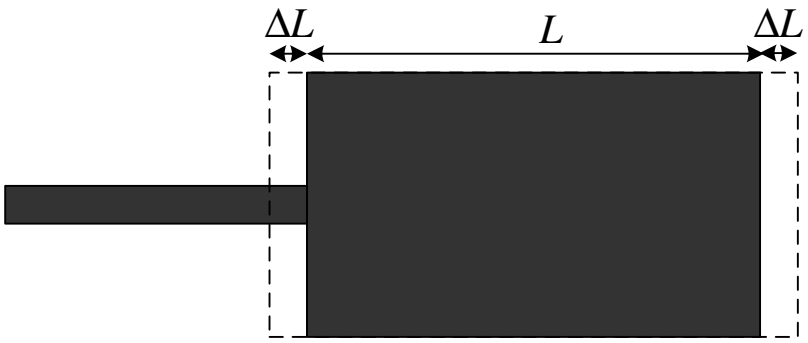

B. Resonant frequency of the dominant TM_{001} mode

$$L_{eff} = \frac{\lambda_0}{2} = \frac{v}{2f^{(001)}} = \frac{c}{2\sqrt{\varepsilon_{r_{eff}}}\, f^{(001)}} \Rightarrow f_r^{(001)} = \frac{c}{2L_{eff}\sqrt{\varepsilon_{r_{eff}}}} \qquad (21.3)$$

The resonant frequency of a patch is sensitive to L, therefore, the exact calculation of L_{eff} is necessary to predict the antenna resonance:

$$\boxed{f_r^{(001)} = \frac{c}{2\sqrt{\varepsilon_{r_{eff}}}\,(L + 2\Delta L)}}. \qquad (21.4)$$

The field of the TM_{001} mode does not depend on the x and y coordinates but it strongly depends on the z coordinate, along which a standing wave is formed due to the patch begin and end edges being terminated with almost ideal open-circuit loads. The figure below shows the vertical **E**-field distribution along z when the patch is in resonance.

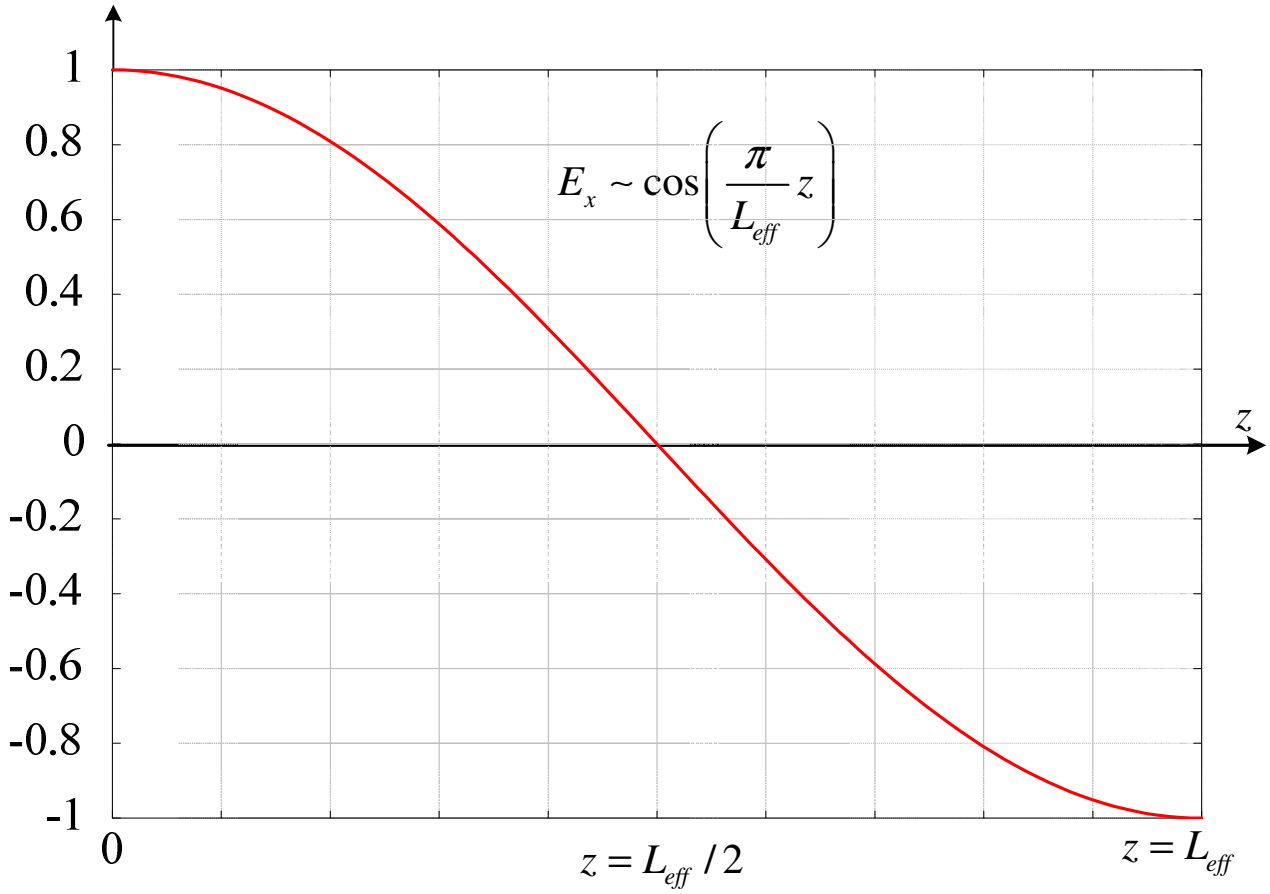

C. The patch width W

$$W = \frac{1}{2f_r\sqrt{\mu_0\varepsilon_0}}\sqrt{\frac{2}{\varepsilon_r+1}} = \frac{c}{2f_r}\sqrt{\frac{2}{\varepsilon_r+1}} \tag{21.5}$$

Expression (21.5) makes the width W equal to about half a wavelength. It leads to good radiation efficiencies and acceptable dimensions.

D. Equivalent circuit of the patch

The dominant TM_{001} mode has a uniform field distribution along the y-axis at the slots formed at the begin and end edges of the patch. The equivalent conductance G of each slot is obtained from the theory of uniform apertures (see Lecture 17) while the slot susceptance B is obtained from the fringe capacitance. The slot conductance and susceptance can be calculated as:

$$G = \frac{W}{120\lambda_0}\left[1-\frac{1}{24}\left(\frac{2\pi h}{\lambda_0}\right)^2\right], \quad \text{for } \frac{h}{\lambda_0} < \frac{1}{10}, \tag{21.6}$$

$$B = \frac{W}{120\lambda_0}\left[1-0.636\ln\left(\frac{2\pi h}{\lambda_0}\right)^2\right], \quad \text{for } \frac{h}{\lambda_0} < \frac{1}{10}. \tag{21.7}$$

The limitation $(h/\lambda_0) < 0.1$ is necessary since a uniform field distribution along the x-axis (vertical axis) is assumed. The patch has two radiating slots (see the figure below).

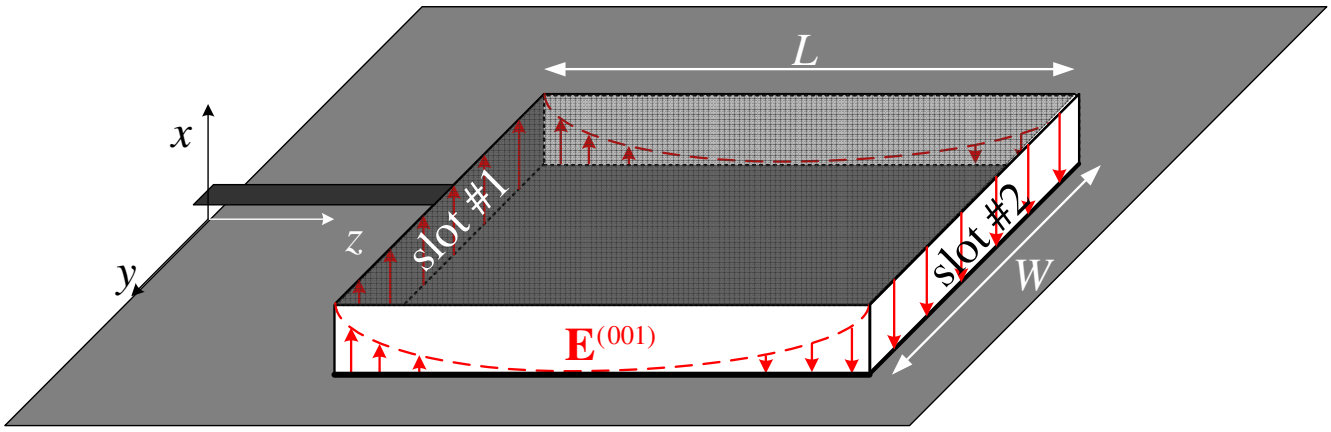

The equivalent circuit of a slot is constructed as a parallel *R*-*C* (*G*-*B*) circuit, using the values computed by (21.6) and (21.7):

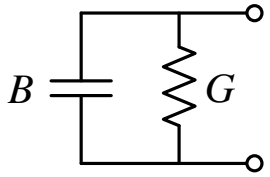

$G = 1/R$ represents the radiation loss, whereas $B = j\omega C$ is the equivalent susceptance, which represents the capacitance of the slot.

More accurate values for the conductance *G* can be obtained through the cavity model:

$$G = I/(120\pi^2), \tag{21.8}$$

where

$$I = \int_0^{\pi} \left[\frac{\sin\left(0.5 k_0 W \cos\theta\right)}{\cos\theta} \right]^2 \sin^3\theta d\theta = -2 + \cos X + X \cdot S_i(X) + \frac{\sin X}{X}, \tag{21.9}$$

and $X = k_0 W$, $k_0 = \omega\sqrt{\mu_0 \varepsilon_0}$. S_i denotes the sine integral, $S_i(x) = \int_0^x (\sin y)/y dy$.

The equivalent circuit representing the whole patch in the TM_{001} mode includes the two radiating slots as parallel *R*-*C* circuits and the patch connecting them as a transmission line, the characteristics of which are computed in the same way as those of a microstrip line.

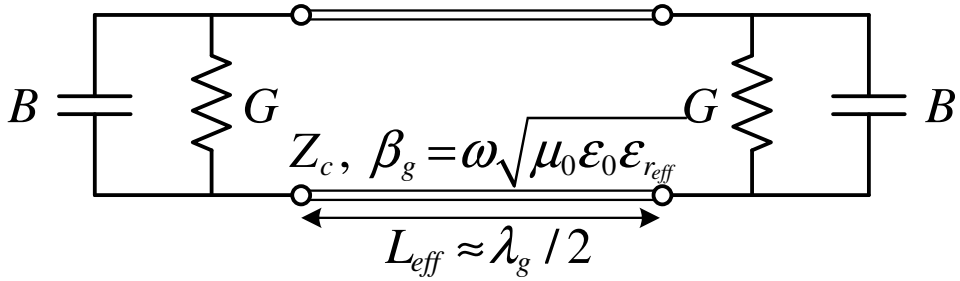

Here, Z_c is the characteristic impedance of the patch-equivalent microstrip line and β_g is its phase constant. When the losses are not negligible, we must include also the attenuation constant α (see Lecture 20).

E. Resonant input resistance

When the patch is resonant, the susceptances of both slots cancel out at the feed point regardless of the position of the feed along the patch. Thus, the input admittance is always purely real. This real value, however, strongly depends on the feed position along z. This is easily shown on the Smith chart for the admittance transformation through a transmission line.

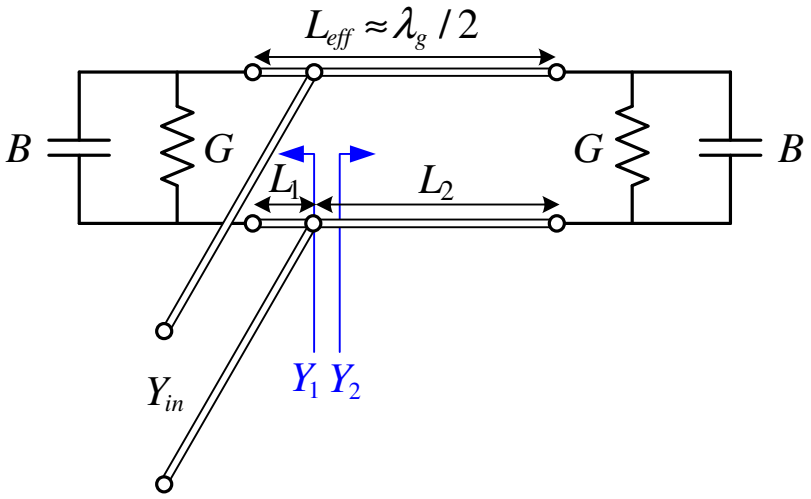

At the feed point, the impedance of each slot is transformed by the respective transmission line representing a portion of the patch:

$$Y_{in} = Y_1 + Y_2 \tag{21.10}$$

The admittance transformation is given by

$$Y_{in} = Y_c \left[\frac{Y_L + jY_c \tan(\beta_g L)}{Y_c + jY_L \tan(\beta_g L)} \right] = Y_L\big|_{\beta_g L = \pi}, \quad Y_c = Z_c^{-1} \tag{21.11}$$

if the line is loss-free. Below, the Smith charts illustrate the slot-impedance transformations and their addition, which produces a real normalized admittance, in three cases: (1) the patch is fed at one edge ($L_1 = 0$, $L_2 = L$), (2) the patch is fed at the center ($L_1 = L_2 = L/2$), and (3) the patch is fed at a distance (feed inset) $z_0 = 0.165\lambda$.

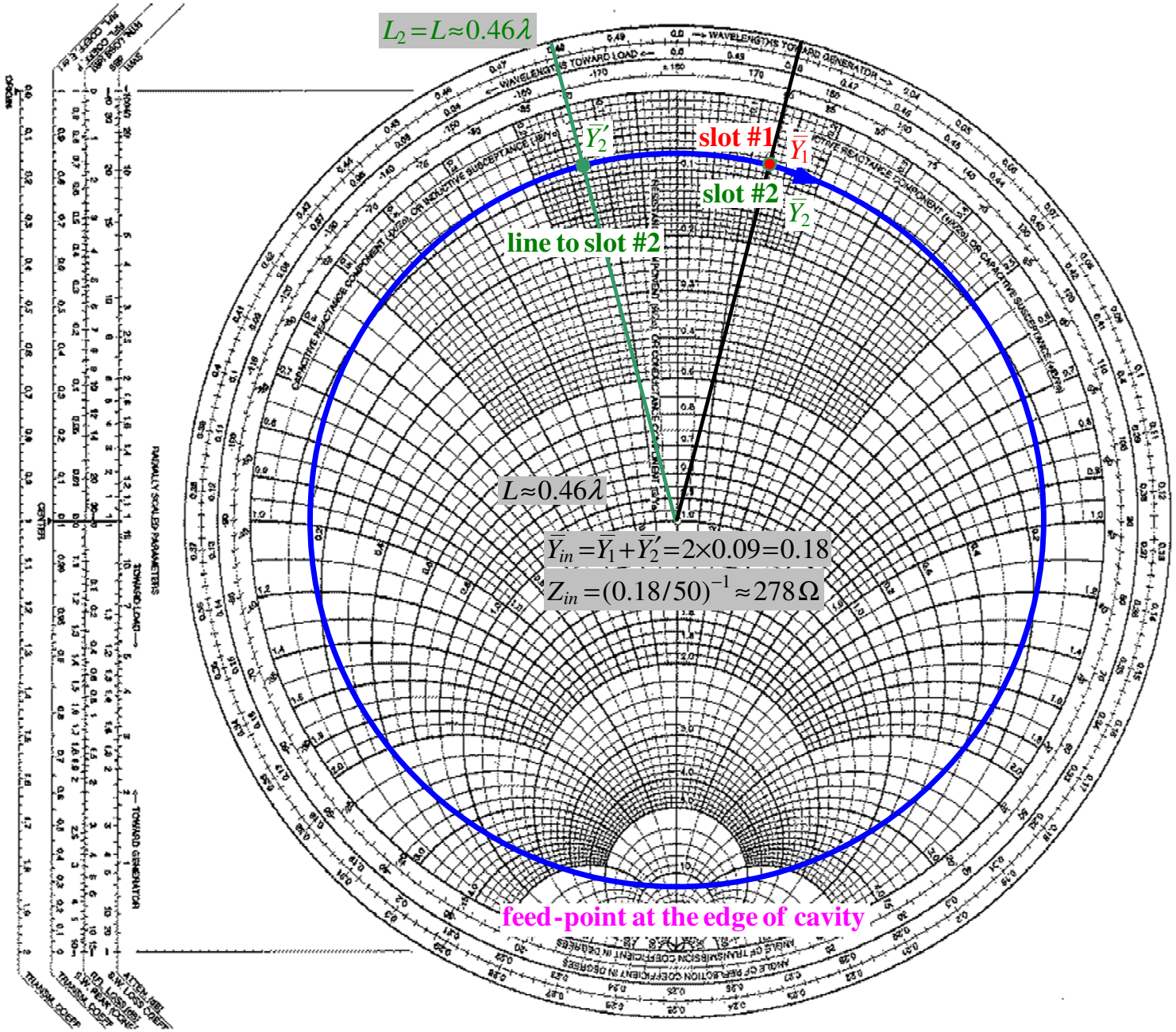
$L_2 = L \approx 0.46\lambda$
$\bar{Y}_2'$
slot #1
$\bar{Y}_1$
slot #2
$\bar{Y}_2$
line to slot #2
$L \approx 0.46\lambda$
$Y_{in} = Y_1 + Y_2' = 2 \times 0.09 = 0.18$
$Z_{in} = (0.18/50)^{-1} \approx 278\,\Omega$
feed-point at the edge of cavity

Smith Chart

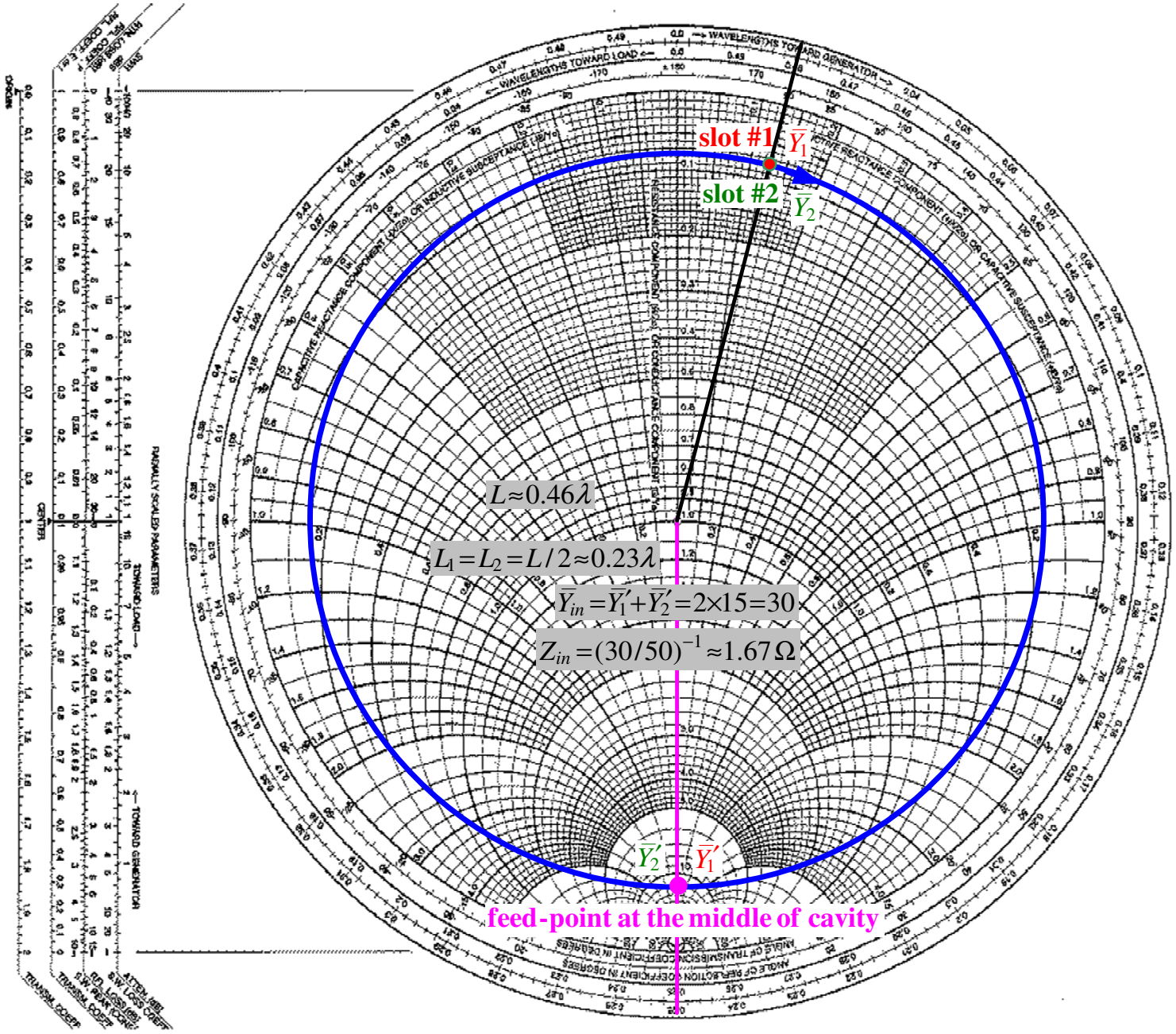
slot #1
$\bar{Y}_1$
slot #2
$\bar{Y}_2$
$L \approx 0.46\lambda$
$L_1 = L_2 = L/2 \approx 0.23\lambda$
$\bar{Y}_{in} = \bar{Y}_1' + \bar{Y}_2' = 2 \times 15 = 30$
$Z_{in} = (30/50)^{-1} \approx 1.67\,\Omega$
$\bar{Y}_2'$
$\bar{Y}_1'$
feed-point at the middle of cavity

Smith Chart

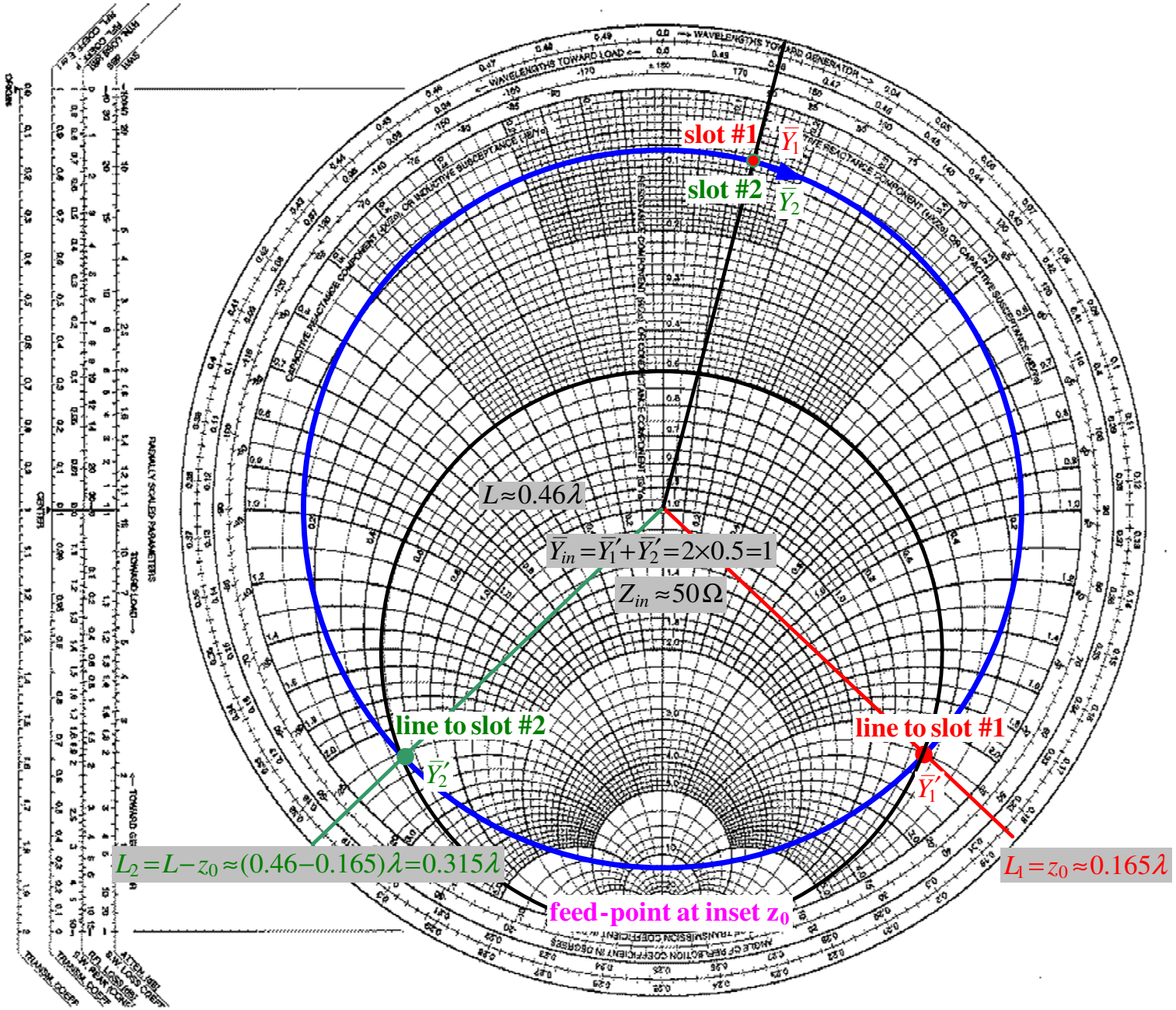
slot #1
$\bar{Y}_1$
slot #2
$\bar{Y}_2$
$L \approx 0.46\lambda$
$\bar{Y}_{in} = \bar{Y}_1' + \bar{Y}_2' = 2 \times 0.5 = 1$
$Z_{in} \approx 50\,\Omega$
line to slot #2
line to slot #1
$\bar{Y}_2'$
$\bar{Y}_1'$
$L_2 = L - z_0 \approx (0.46 - 0.165)\lambda = 0.315\lambda$
$L_1 = z_0 \approx 0.165\lambda$
feed-point at inset z_0

Smith Chart

The edge feed and the inset feed are illustrated below.

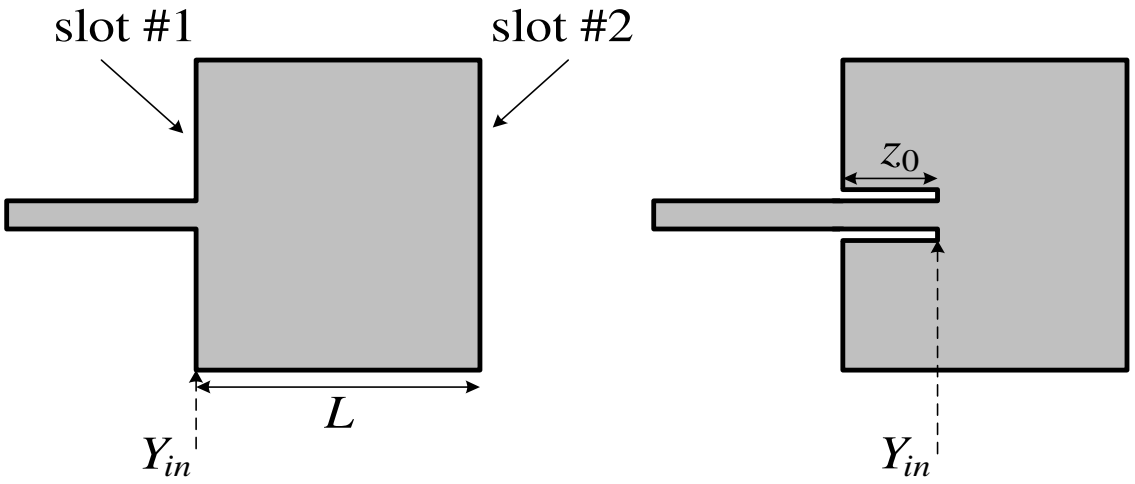

The two slots are separated by an electrical distance of 180°. However, because of the fringe effect the physical length L is slightly less than $\lambda/2$. The reduction of the length is not much. Typically, it is $0.48\lambda \le L \le 0.49\lambda$.

Ideally, the resonant input impedance of the patch for the dominant TM_{001} mode is entirely resistive and equal to half the transformed resistance of each slot:

$$Z_{in} = \frac{1}{Y_{in}} = \frac{1}{2G_1'} = R_{in}. \tag{21.12}$$

In reality, there is some mutual influence between the two slots, described by a mutual conductance and it should be included for more accurate calculations:

$$R_{in} = \frac{1}{2(G_1' \pm G_{12})}, \tag{21.13}$$

where the "+" sign relates to the odd modes, while the "–" sign relates to the even modes. Normally, $G_{12} \ll G_1'$.

For most patch antennas fed at the edge, R_{in} is greater than the characteristic impedance Z_c of the microstrip feed line (typically Z_c = 50 to 75 Ω). That is why, the inset-feed technique is widely used to achieve impedance match.

The figure below illustrates the normalized input impedance of a 1-D (along the y axis) loss-free open-ended transmission-line, the behavior of which is very close to that of the dominant mode of the patch.

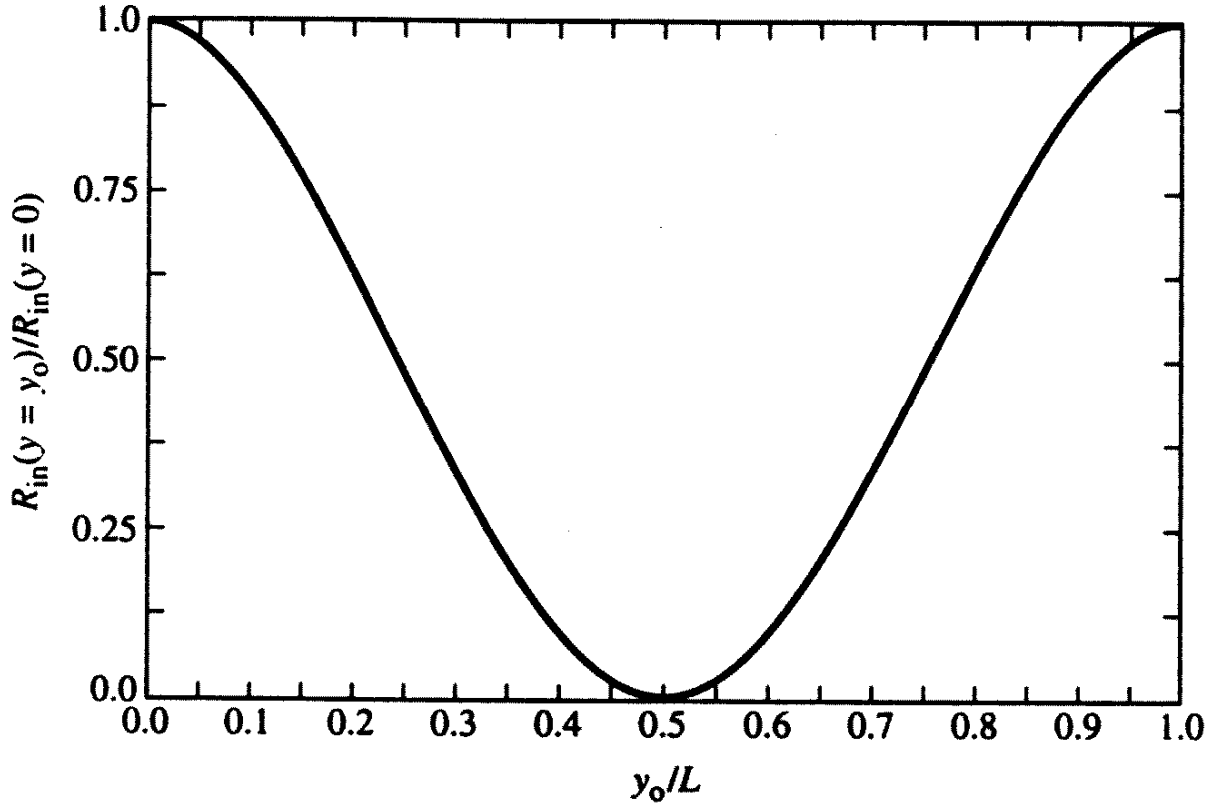

Fig 14.14, pp 735, C. Balanis

Using modal expansion, the input resistance for the inset-feed at $z = z_0$ is given approximately by

$$R_{in}(z_0)=\frac{1}{2\left(G_1 \pm G_{12}\right)}\left[\cos^2\left(\frac{\pi}{L}z_0\right)+\frac{G_1^2+B_1^2}{Y_c^2}\sin^2\left(\frac{\pi}{L}z_0\right)-\frac{B_1}{Y_c}\sin\left(\frac{2\pi}{L}z_0\right)\right] \quad (21.14)$$

Here, G_1 and B_1 are calculated using (21.6) and (21.7). For most feeding microstrips, $G_1 / Y_c \ll 1$ and $B_1 / Y_c \ll 1$. Then,

$$R_{in}(z_0) \approx \frac{1}{2\left(G_1 \pm G_{12}\right)}\cos^2\left(\frac{\pi}{L}z_0\right) = R_{in(z=0)}\cos^2\left(\frac{\pi}{L}z_0\right). \quad (21.15)$$

Notice that the inset feeding technique for impedance match of the microstrip antennas is conceptually analogous to the off-center or asymmetrical feeding techniques for dipoles. In both cases, a position is sought along a resonant structure, where the current magnitude has the desired value.

2. Designing a Rectangular Patch Using the Transmission Line Model

Input data: ε_r, h, f_r

1) Calculate W using (21.5).
2) Calculate ε_{reff} using (21.5) and equation (6) from Lecture 20.
3) Calculate the extension ΔL due to the fringing effect using (21.1).
4) Calculate the actual (physical) length of the patch using

$$L = \frac{\lambda_0}{2} - 2\Delta L \text{ or } L = \frac{1}{2 f_r \sqrt{\varepsilon_{reff}} \sqrt{\mu_0 \varepsilon_0}} - 2\Delta L. \qquad (21.16)$$

5) Calculate radiating slot admittance using (21.6) and (21.7).
6) Calculate resonant input resistance at patch edge using (21.12) or (21.13) with $G_1' = G$ from (21.6).
7) If R_{in} calculated in step 6 is too large, calculate the inset distance z_0 using (21.14) or (21.15).

3. Cavity Model for the Rectangular Patch

The TL model is very limited in its description of the real processes taking place when a patch is excited. It takes into account only the TM^x_{00n} modes where the energy propagates only in the longitudinal z direction. The field distribution along the x and y axes is assumed uniform. It is true that the dominant TM^x_{001} is prevalent but the performance of the patch is also affected by higher-order modes.

The cavity model is a more general model of the patch which imposes open-end conditions at the side edges of the patch. It represents the patch as a dielectric-loaded cavity with:

- electrical walls (top and bottom), and
- magnetic walls (around the perimeter of the patch.

The magnetic wall is a wall at which

$$\hat{\mathbf{n}} \times \mathbf{H} = 0 \quad \text{(the } \mathbf{H}\text{-field is purely normal)}$$

$$\hat{\mathbf{n}} \cdot \mathbf{E} = 0 \quad \text{(the } \mathbf{E}\text{-field is purely tangential)}$$

It is analogous to the open end termination in the theory of transmission lines.

If we treat the microstrip antenna only as a cavity, we cannot represent

radiation because an ideal loss-free cavity does not radiate and its input impedance is purely reactive. To account for the radiation, a loss mechanism is introduced. This is done by introducing an effective loss tangent, δ_{eff}.

The thickness of the substrate is very small. The waves generated and propagating beneath the patch undergo considerable reflection at the edges of the patch. Only a very small fraction of them is being radiated. The cavity model assumes that the **E** field is purely tangential to the slots formed between the ground plane and the patch edges (magnetic walls). Moreover, it considers only TM^x modes, i.e., modes with no H_x component. These assumptions are, basically, very much true.

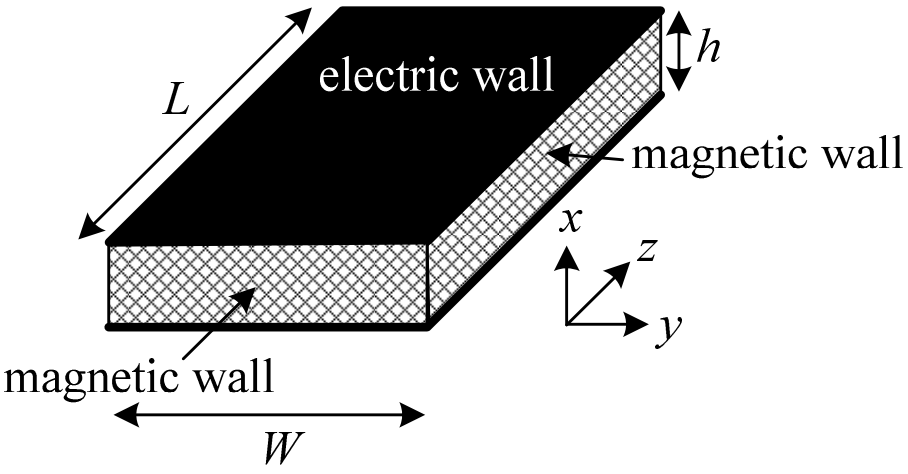

The TM^x modes are fully described by a single scalar function A_x – the x-component of the magnetic vector potential:

$$\mathbf{A} = A_x \hat{\mathbf{x}}. \tag{21.17}$$

In a homogeneous source-free medium, A_x satisfies the wave equation:

$$\nabla^2 A_x + k^2 A_x = 0. \tag{21.18}$$

For regular shapes (like the rectangular cavity), it is advantageous to use the separation of variables:

$$\frac{\partial^2 A_x}{\partial x^2} + \frac{\partial^2 A_x}{\partial y^2} + \frac{\partial^2 A_x}{\partial z^2} + k^2 A_x = 0 \tag{21.19}$$

$$A_x = X(x)Y(y)Z(z) \tag{21.20}$$

$$YZ\frac{\partial^2 X}{\partial x^2}+XZ\frac{\partial^2 Y}{\partial x^2}+XY\frac{\partial^2 Z}{\partial x^2}=-k^2XYZ$$

$$\frac{1}{X}\frac{\partial^2 X}{\partial x^2}+\frac{1}{Y}\frac{\partial^2 Y}{\partial y^2}+\frac{1}{Z}\frac{\partial^2 Z}{\partial z^2}=-k^2 \tag{21.21}$$

$$\frac{d^2X}{dx^2}+k_x^2X=0,\ \frac{d^2Y}{dy^2}+k_y^2Y=0,\ \frac{d^2Z}{dz^2}+k_z^2Z=0 \tag{21.22}$$

The eigenvalue equation is

$$k_x^2+k_y^2+k_z^2=k^2. \tag{21.23}$$

The solutions of (21.22) are harmonic functions:

$$\begin{aligned} X(x)&=\sum_n A_n^c\cos(k_{xn}x)+A_n^s\sin(k_{xn}x),\\ Y(y)&=\sum_n B_n^c\cos(k_{yn}y)+B_n^s\sin(k_{yn}y),\\ Z(z)&=\sum_n C_n^c\cos(k_{zn}z)+C_n^s\sin(k_{zn}z). \end{aligned} \tag{21.24}$$

When the functions in (21.24) are substituted in (21.20), they give the general solution of (21.18). The particular solution of (21.18) depends on the boundary conditions.

In our case, there are electric walls at $x=0$ and $x=h$. There, the tangential **E**-field components must vanish, i.e., $E_y=E_z=0\big|_{x=0,h}$. Having in mind that

$$E_x=\frac{1}{j\omega\mu\varepsilon}\left(\frac{\partial^2 A_x}{\partial x^2}+k^2A_x\right),\ E_y=\frac{1}{j\omega\mu\varepsilon}\left(\frac{\partial^2 A_x}{\partial x\partial y}\right),\ E_z=\frac{1}{j\omega\mu\varepsilon}\left(\frac{\partial^2 A_z}{\partial x\partial z}\right), \tag{21.25}$$

we set A_x at the top and bottom walls as

$$\left.\frac{\partial A_x}{\partial x}\right|_{x=0,h}=0. \tag{21.26}$$

At all side walls, we set a vanishing normal derivative for A_x:

$$\left.\frac{\partial A_x}{\partial z}\right|_{z=0,L}=0,\ \left.\frac{\partial A_x}{\partial y}\right|_{y=0,W}=0. \tag{21.27}$$

This ensures vanishing H_x and H_y at $z=0$ and $z=L$, as well as vanishing H_x and H_z at $y=0$ and $y=W$ (magnetic walls), as follows from the relation between the **H**-field and A_x,

$$H_x = 0,\ H_y = \frac{1}{\mu}\left(\frac{\partial A_x}{\partial z}\right),\ H_x = \frac{1}{\mu}\left(\frac{\partial A_x}{\partial y}\right). \tag{21.28}$$

It is now obvious that the solution must appear in terms of the functions

$$\begin{aligned} X(x) &= \sum_n A_n^c \cos(k_{xn}x),\ k_{xn} = n\frac{\pi}{h}, \\ Y(y) &= \sum_n B_n^c \cos(k_{yn}y),\ k_{yn} = n\frac{\pi}{W}, \\ Z(z) &= \sum_n C_n^c \cos(k_{zn}z),\ k_{zn} = n\frac{\pi}{L}. \end{aligned} \tag{21.29}$$

The spectrum of the eigenmodes in the cavity is discrete. The frequencies of those modes (the resonant frequencies) can be calculated from (21.23) as

$$\left(\frac{m\pi}{h}\right)^2 + \left(\frac{n\pi}{W}\right)^2 + \left(\frac{p\pi}{L}\right)^2 = \left(\omega_r^{(mnp)}\right)^2 \mu\varepsilon, \tag{21.30}$$

$$\boxed{f_r^{(mnp)} = \frac{1}{2\pi\sqrt{\mu\varepsilon}}\sqrt{\left(\frac{m\pi}{h}\right)^2 + \left(\frac{n\pi}{W}\right)^2 + \left(\frac{p\pi}{L}\right)^2}}. \tag{21.31}$$

The mode with the lowest resonant frequency is the ***dominant mode***. Since usually $L > W$, the lowest-frequency mode is the TM_{001}^x mode, for which

$$f_r^{(001)} = \frac{1}{2\pi\sqrt{\mu\varepsilon}}\frac{\pi}{L} = \frac{c}{2L\sqrt{\varepsilon_r}}. \tag{21.32}$$

The dominant TM_{001}^x mode is exactly the mode considered by the transmission-line model (see previous sections). The field distribution of some low-order modes is given in the following figure.

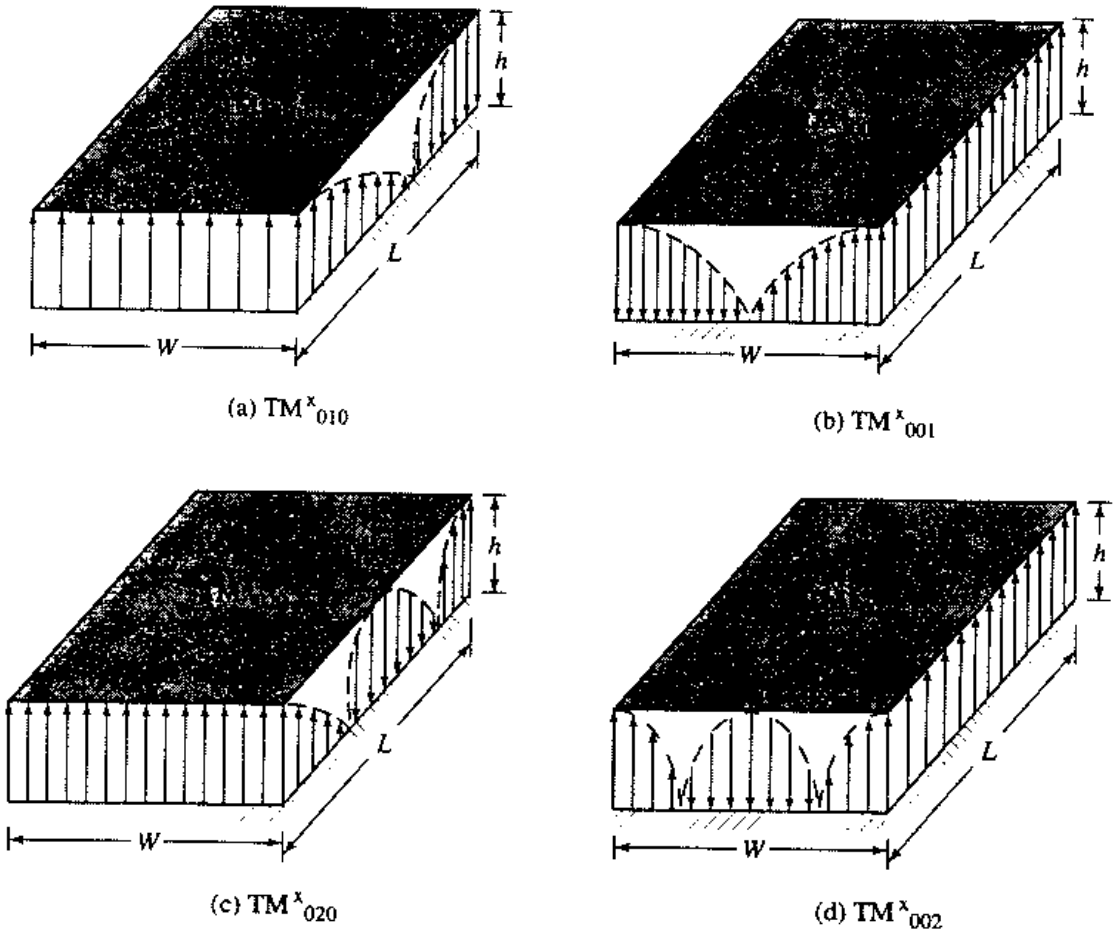

Fig. 14.13, pp. 741, Balanis

The general solution for the $A_x^{(mnp)}$ [see (21.20) and (21.24)] is

$$A_x^{(mnp)} = \left[A_x^c \cos\left(m\frac{\pi}{h}x \right) \right] \left[B_x^c \cos\left(n\frac{\pi}{W}y \right) \right] \left[C_x^c \cos\left(p\frac{\pi}{L}z \right) \right], \quad (21.33)$$

or

$$A_x^{(mnp)} = A_{mnp} \cdot \cos\left(m\frac{\pi}{h}x \right) \cdot \cos\left(n\frac{\pi}{L}y \right) \cdot \cos\left(p\frac{\pi}{W}z \right). \quad (21.34)$$

The respective field solution for the (m,n,p) mode is

$$E_x = -j\frac{(k^2 - k_x^2)}{\omega\mu\varepsilon} A_{mnp} \cdot \cos(k_x x) \cdot \cos(k_y y) \cdot \cos(k_z z), \quad (21.35)$$

$$E_y = -j\frac{k_x k_y}{\omega\mu\varepsilon} A_{mnp} \cdot \sin(k_x x) \cdot \sin(k_y y) \cdot \cos(k_z z), \quad (21.36)$$

$$E_z = -j\frac{k_x k_z}{\omega\mu\varepsilon} A_{mnp} \cdot \sin(k_x x) \cdot \cos(k_y y) \cdot \sin(k_z z), \tag{21.37}$$

$$H_x = 0, \tag{21.38}$$

$$H_y = -\frac{k_z}{\mu} A_{mnp} \cdot \cos(k_x x) \cdot \cos(k_y y) \cdot \sin(k_z z), \tag{21.39}$$

$$H_z = \frac{k_y}{\mu} A_{mnp} \cdot \cos(k_x x) \cdot \sin(k_y y) \cdot \cos(k_z z). \tag{21.40}$$

For the dominant TM_{001}^{x} mode,

$$E_x = \left[-j(k^2 - \pi^2 / h^2) / (\omega\mu\varepsilon)\right] A_{001} \cos(\pi z / L),\ E_y = E_z = 0, \tag{21.41}$$

$$H_y = -(\pi / \mu L) A_{001} \sin(\pi z / L),\ H_x = H_z = 0. \tag{21.42}$$

4. Cavity Model for the Radiated Field of a Rectangular Patch

The microstrip patch is represented by the cavity model reasonably well assuming that the material of the substrate is truncated and does not extend beyond the edges of the patch. The four side walls (the magnetic walls) represent four narrow apertures (slots) through which radiation takes place.

The equivalence principle is used to calculate the radiation fields. The field inside the cavity is assumed equal to zero, and its influence on the field in the infinite region outside is represented by the equivalent surface currents on the surface of the cavity.

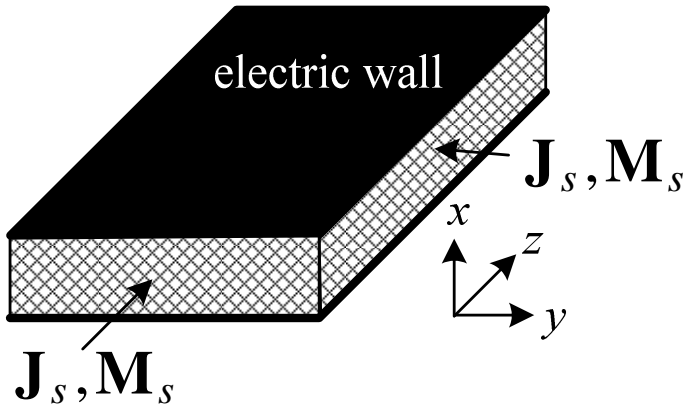

$$\mathbf{J}_s = \hat{\mathbf{n}} \times \mathbf{H}$$

$$\mathbf{M}_s = -\hat{\mathbf{n}} \times \mathbf{E}$$

Because of the very small height h of the substrate, the field is concentrated beneath the patch. There is some actual electrical current at the top metallic plate, however, its contribution to radiation is negligible. That is because: (1) it is backed by a conductor, and (2) it is very weak compared to the equivalent currents at the slots. The actual electrical current density of the top patch is maximum at the edges of the patch.

In the cavity model, the side walls employ magnetic-wall boundary condition, which sets the tangential **H** components at the slots equal to zero. Therefore, the equivalent surface current density is zero:

$$\mathbf{J}_s = \hat{\mathbf{n}} \times \mathbf{H} = 0. \tag{21.43}$$

Only the equivalent magnetic current density

$$\mathbf{M}_s = -\hat{\mathbf{n}} \times \mathbf{E} \tag{21.44}$$

contributes to the radiated field.

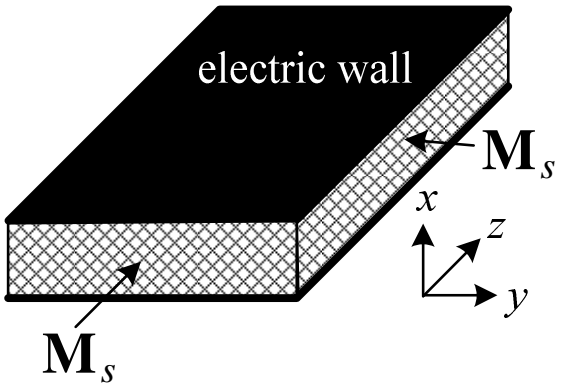

$$\mathbf{J}_s = 0$$
$$\mathbf{M}_s = -2\hat{\mathbf{n}} \times \mathbf{E}$$

The influence of the infinite ground plane is accounted for by the image theory, according to which the currents $\mathbf{M}_s$ in the presence of the infinite plane radiate as if magnetic currents of double strength radiate in free space:

$$\mathbf{M}_s = -2\hat{\mathbf{n}} \times \mathbf{E}. \tag{21.45}$$

Note that an E_x field at the slots corresponds to $\mathbf{M}_s$ density vector, which is tangential to the ground plane. Thus, its image is of the same direction. The equivalent magnetic current densities for the dominant TM_{001}^{x} mode are sketched below.

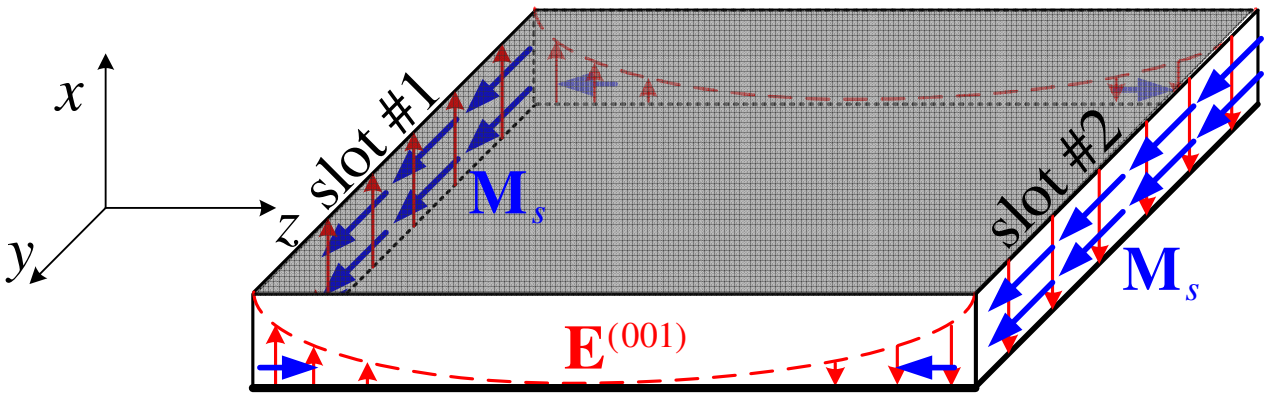

At slots #1 and #2, the equivalent $\mathbf{M}_s$ currents are co-directed and with equal amplitudes. They are constant along x and y.

Radiation from a slot with constant current density

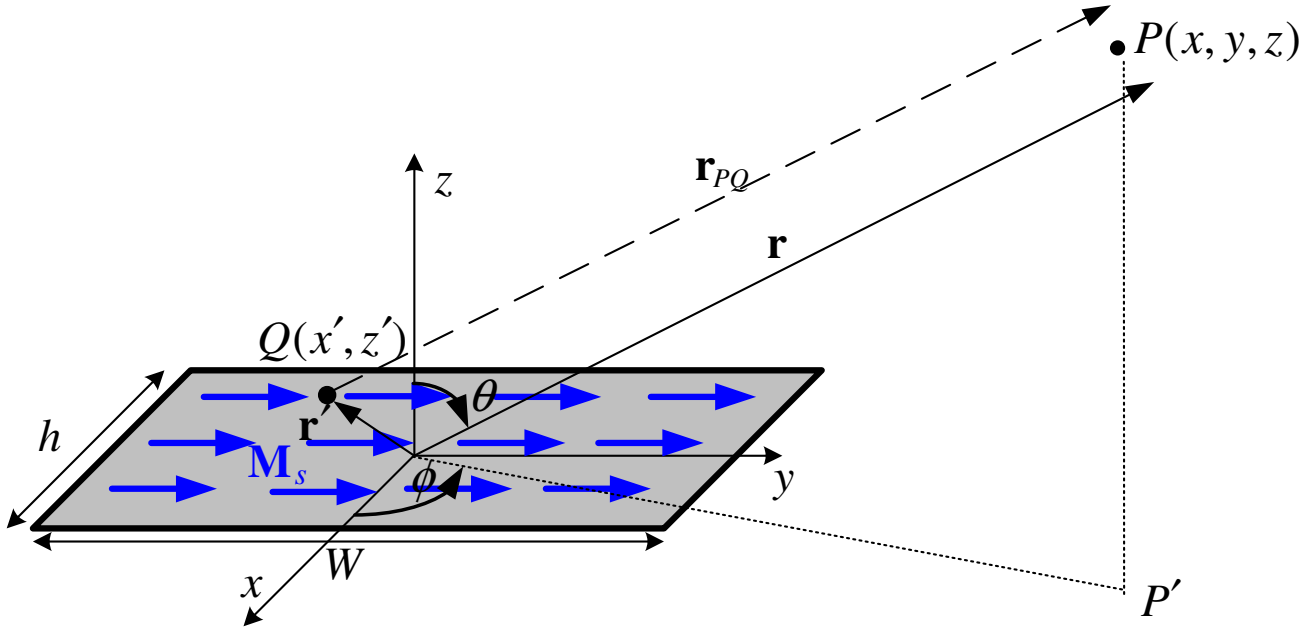

The radiation from an (x-y) slot of constant $\mathbf{M}_s$ currents is found using the electric vector potential $\mathbf{F}$. Since $\mathbf{M}_s$ has only a y component, so does $\mathbf{F}$: $\mathbf{F} = F_y \hat{\mathbf{y}}$.

$$F_y(r,\theta,\phi) = \frac{\varepsilon}{4\pi} \int_{-h/2}^{h/2} \int_{-W/2}^{W/2} \frac{M_y}{r_{PQ}} e^{-jk_0 r_{PQ}} dx' dy'. \qquad (21.46)$$

Here, $M_y = -2E_0$, E_0 being the phasor of the **E**-field at the radiating slot, and $r_{PQ} = r - \mathbf{r}' \cdot \hat{\mathbf{r}} = r - x' \sin\theta\cos\phi - y' \sin\theta\sin\phi$.

$$F_y = -2\varepsilon E_0 \frac{e^{-jk_0 r}}{4\pi r} \int_{-h/2}^{h/2} \exp(jk_0 x' \sin\theta\cos\phi)dx' \cdot \int_{-W/2}^{W/2} \exp(jk_0 y' \sin\theta\sin\phi)dy' \quad (21.47)$$

$$\Rightarrow F_y = -\frac{\varepsilon E_0 Wh}{2\pi r} \cdot e^{-jk_0 r} \cdot \frac{\sin X}{X} \cdot \frac{\sin Y}{Y} \quad (21.48)$$

where

$$X = \frac{k_0 h}{2} \sin\theta\cos\phi,$$

$$Y = \frac{k_0 W}{2} \sin\theta\sin\phi.$$

According to the relation between the far-zone **E**-field and the vector potential,

$$E_r \approx 0,\ E_\phi = j\omega\eta F_\theta,\ E_\theta = -j\omega\eta F_\phi, \quad (21.49)$$

where $\eta = \sqrt{\mu_0 / \varepsilon_0}$, $F_\theta = F_y \cos\theta\sin\phi$, and $F_\phi = F_y \cos\phi$.

$$\Rightarrow E_\phi = j\omega\eta\varepsilon_0 \frac{WhE_0}{2\pi r} e^{-jk_0 r} \cos\theta\sin\phi \frac{\sin X}{X} \frac{\sin Y}{Y}, \quad (21.50)$$

$$\Rightarrow E_\theta = -j\omega\eta\varepsilon_0 \frac{WhE_0}{2\pi r} e^{-jk_0 r} \cos\phi \frac{\sin X}{X} \frac{\sin Y}{Y}. \quad (21.51)$$

Since $\omega\eta\varepsilon_0 = k_0$,

$$E_\phi = jk_0 W \frac{V_0}{2\pi r} e^{-jk_0 r} \left(\cos\theta\sin\phi \frac{\sin X}{X} \frac{\sin Y}{Y} \right), \quad (21.52)$$

$$E_\theta = -jk_0 W \frac{V_0}{2\pi r} e^{-jk_0 r} \left(\cos\phi \frac{\sin X}{X} \frac{\sin Y}{Y} \right). \quad (21.53)$$

Here $V_0 = hE_0$ is the voltage between the patch edge and the ground plane.

Slots #1 and #2 form an array of two slits with excitation of equal magnitude and phase, separated by the physical distance *L*. Their AF is

$$AF_{12} = 2\cos\left(\frac{k_0 L_{eff}}{2} \cos\theta \right). \quad (21.54)$$

Here $L_{eff} = L + 2\Delta L$ is the effective patch length. Thus, the total radiation field is

$$E_\phi^t = j\frac{k_0 W V_0}{\pi r} e^{-jk_0 r}\left(\cos\theta \sin\phi \frac{\sin X}{X}\frac{\sin Y}{Y}\right)\times\left[\cos\left(\frac{k_0 L_{eff}}{2}\cos\theta\right)\right], \quad (21.55)$$

$$E_\theta^t = -j\frac{k_0 W V_0}{\pi r} e^{-jk_0 r}\left(\cos\phi \frac{\sin X}{X}\frac{\sin Y}{Y}\right)\times\left[\cos\left(\frac{k_0 L_{eff}}{2}\cos\theta\right)\right]. \quad (21.56)$$

Introducing $Z = (k_0 L_{eff}/2)\cos\theta$, the pattern of the patch is obtained as

$$f(\theta,\phi) = \sqrt{\overline{E}_\phi^2 + \overline{E}_\theta^2} = \sqrt{1-\sin^2\phi\cdot\sin^2\theta}\cdot\frac{\sin X}{X}\frac{\sin Y}{Y}\cos Z. \quad (21.57)$$

E-plane pattern (xz plane, $\phi = 0°$, $0° \le \theta \le 180°$)

$$f_E(\theta) = \frac{\sin\left(\frac{k_0 h}{2}\sin\theta\right)}{\frac{k_0 h}{2}\sin\theta}\cdot\cos\left(\frac{k_0 L_{eff}}{2}\cos\theta\right). \quad (21.58)$$

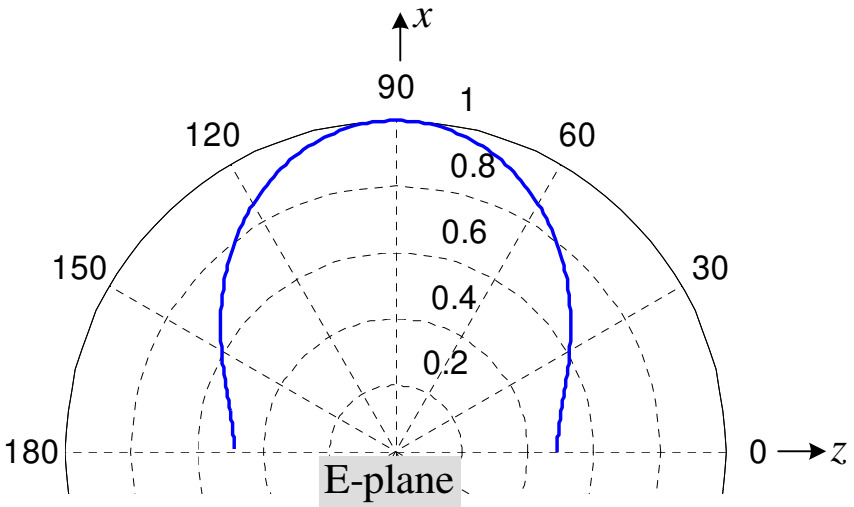

E-plane

$k_0 h = 0.1;\ \varepsilon_r = 2.2$

$L_{eff} = 0.5\lambda_0 / \sqrt{\varepsilon_r}$

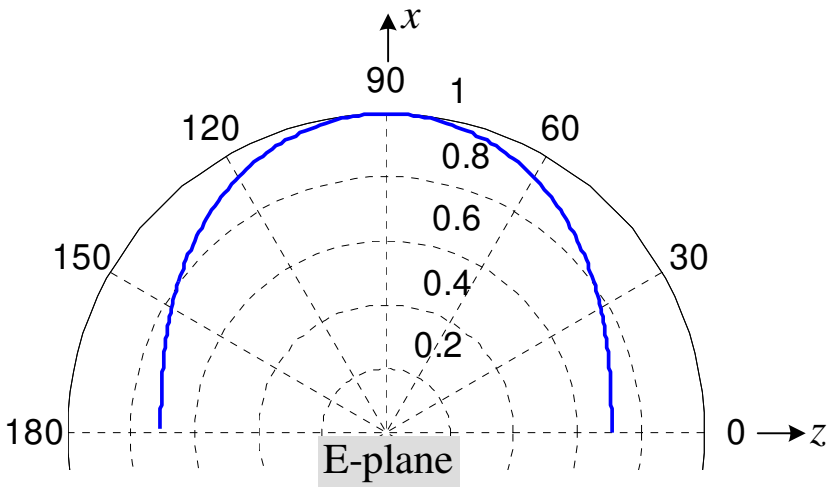

E-plane

$k_0 h = 0.1;\ \varepsilon_r = 4.0$

$L_{eff} = 0.5\lambda_0 / \sqrt{\varepsilon_r}$

H-plane pattern (xy plane, $\theta = 90°$, $0° \le \phi \le 90°$ and $270° \le \phi \le 360°$)

$$f_H(\theta) = \cos\phi \cdot \frac{\sin\left(\frac{k_0 h}{2}\cos\phi\right)}{\frac{k_0 h}{2}\cos\phi} \cdot \frac{\sin\left(\frac{k_0 W}{2}\sin\phi\right)}{\frac{k_0 W}{2}\sin\phi} \qquad (21.59)$$

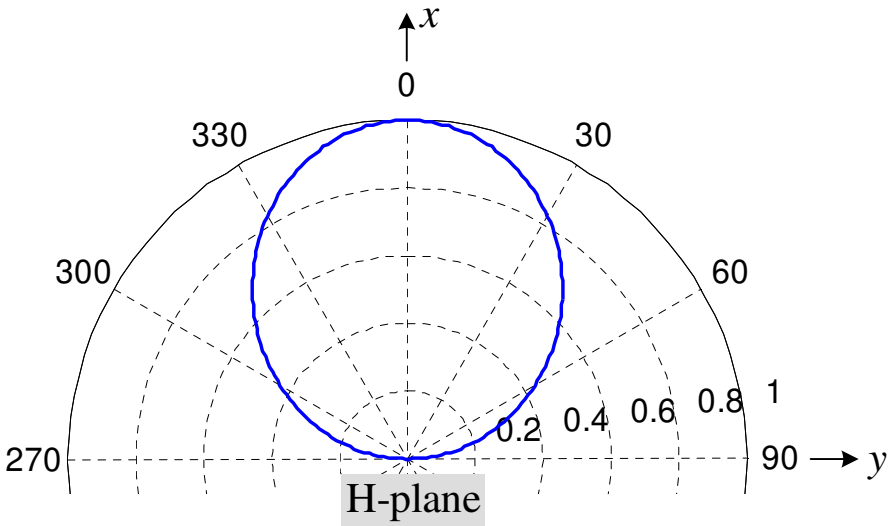

H-plane

$k_0 h = 0.1;\ \varepsilon_r = 2.2$

$W = 0.5\lambda_0 / \sqrt{\varepsilon_r}$

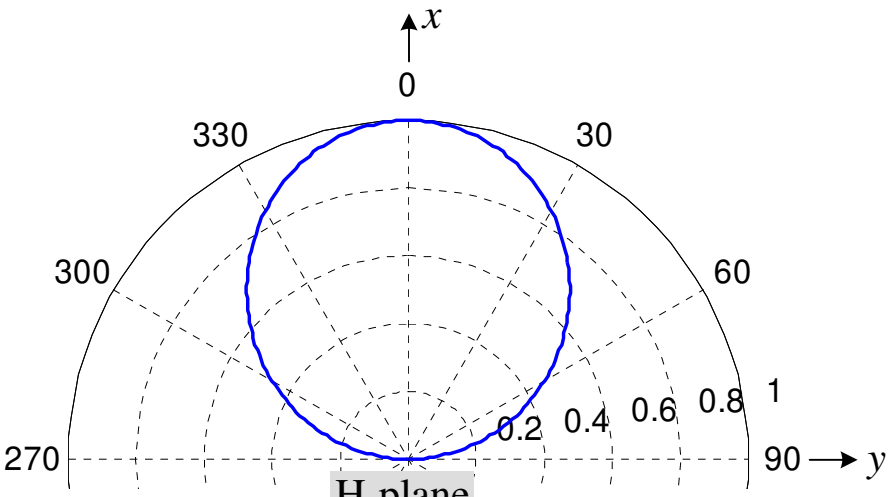

H-plane

$k_0 h = 0.1;\ \varepsilon_r = 4.0$

$W = 0.5\lambda_0 / \sqrt{\varepsilon_r}$

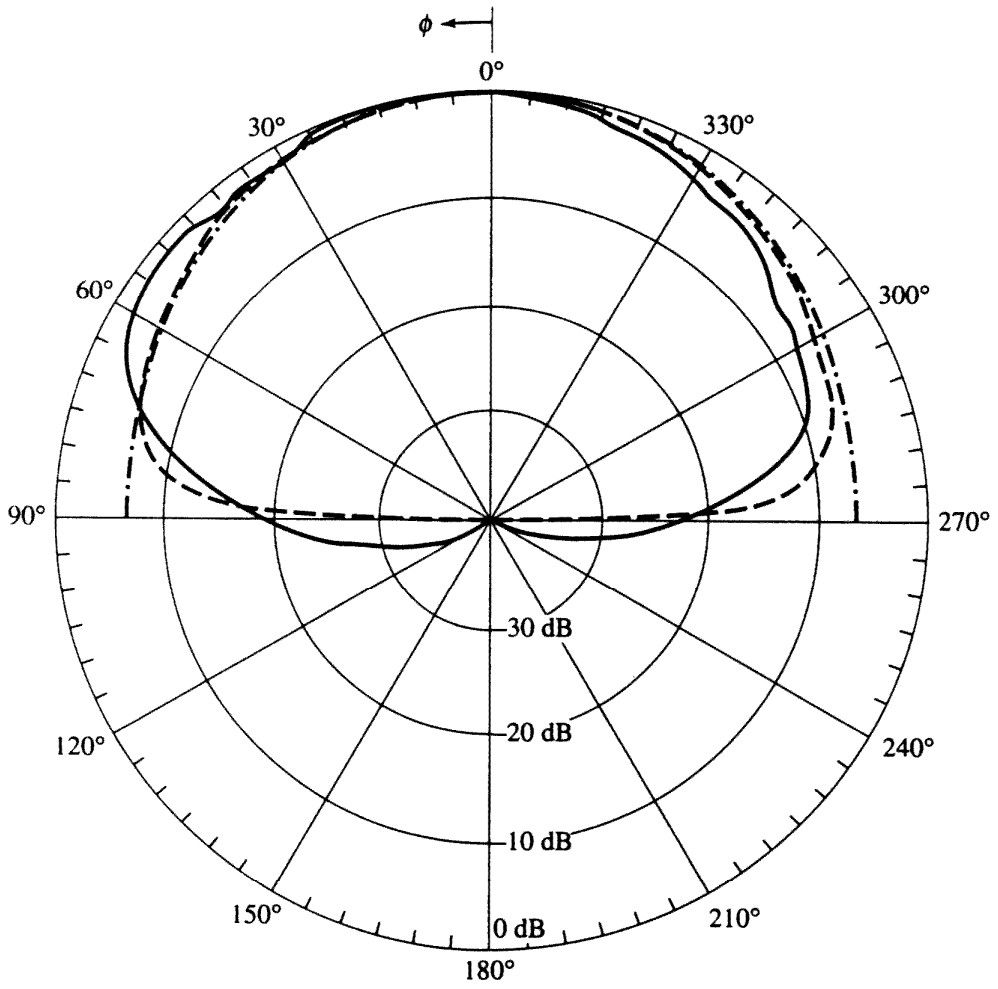

(a) *E*-plane ($\theta = 90°$)

Fig. 14.17, p. 746, Balanis

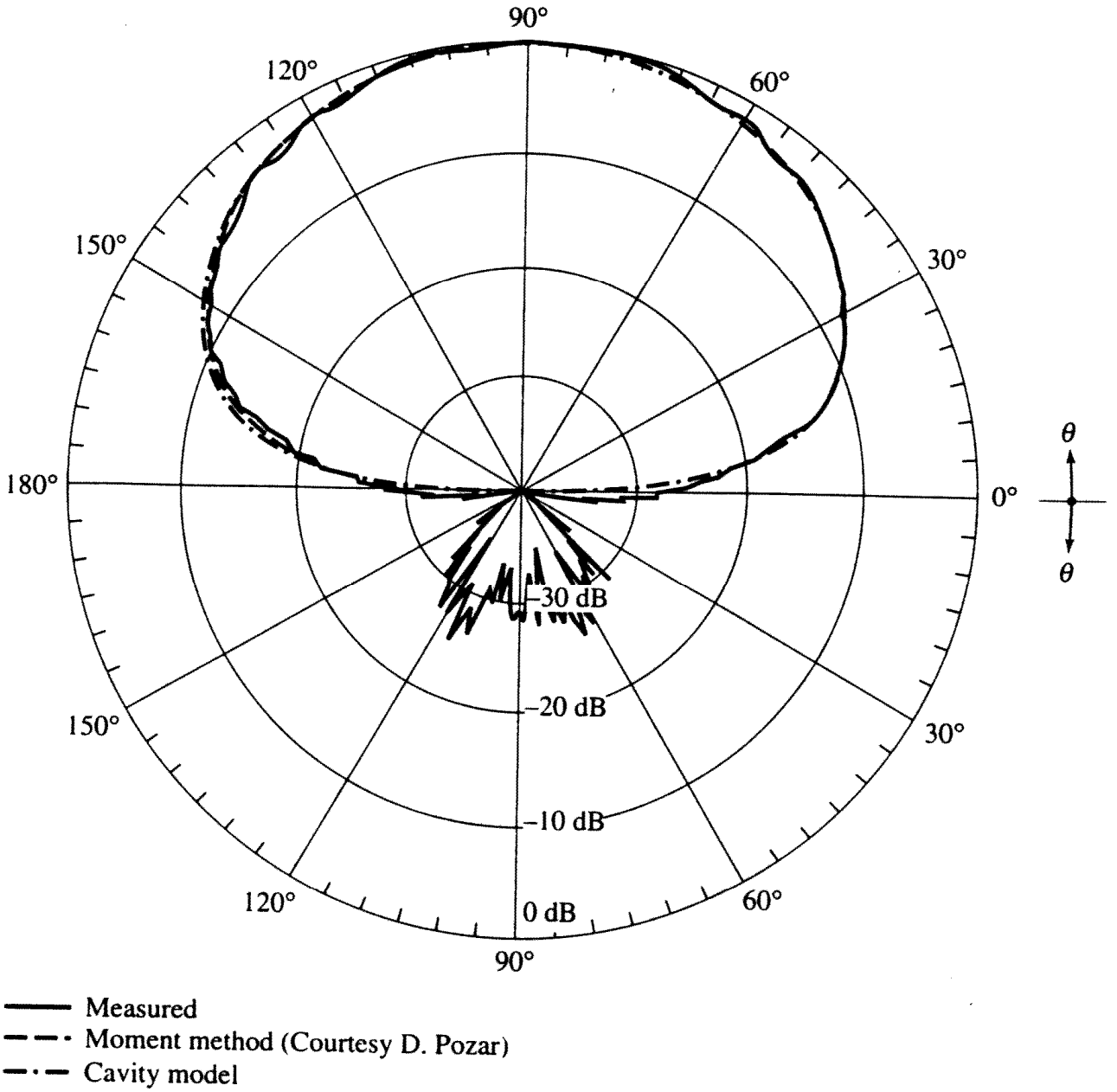

(b) *H*-plane ($\phi = 0°$)

Fig. 14.18, p. 747, Balanis

Non-radiating slots: It can be shown that the slots at $y = -W/2$ and $y = W/2$ do no radiate in the principle **E**- and **H**-planes. In general, these two slots do radiate away from the principle planes, but their field intensity is everywhere small compared to that radiated by slots #1 and #2.